Low-temperature plasma-enhanced atomic layer deposition of 2-D MoS2

Nanoscale

PAPER

View Article Online
View Journal

Cite this: DOI: 10.1039/c8nr02339e

Low-temperature plasma-enhanced atomic layer deposition of 2-D MoS_2: large area, thickness control and tuneable morphology†

Akhil Sharma,[a] Marcel A. Verheijen,[a,b] Longfei Wu,[c] Saurabh Karwal,[a] Vincent Vandalon,[a] Harm C. M. Knoops,[a,d] Ravi S. Sundaram,[d] Jan P. Hofmann,[c] W. M. M. (Erwin) Kessels[a] and Ageeth A. Bol*[a]

Low-temperature controllable synthesis of monolayer-to-multilayer thick MoS_2 with tuneable morphology is demonstrated by using plasma enhanced atomic layer deposition (PEALD). The characteristic self-limiting ALD growth with a growth-per-cycle of 0.1 nm per cycle and digital thickness control down to a monolayer are observed with excellent wafer scale uniformity. The as-deposited films are found to be polycrystalline in nature showing the signature Raman and photoluminescence signals for the mono-to-few layered regime. Furthermore, a transformation in film morphology from in-plane to out-of-plane orientation of the 2-dimensional layers as a function of growth temperature is observed. An extensive study based on high-resolution transmission electron microscopy is presented to unravel the nucleation mechanism of MoS_2 on SiO_2/Si substrates at 450 °C. In addition, a model elucidating the film morphology transformation (at 450 °C) is hypothesized. Finally, the out-of-plane oriented films are demonstrated to outperform the in-plane oriented films in the hydrogen evolution reaction for water splitting applications.

Received 21st March 2018,
Accepted 17th April 2018

DOI: 10.1039/c8nr02339e

rsc.li/nanoscale

1. Introduction

The discovery of graphene and subsequent efforts to thoroughly understand its remarkable physical properties have stimulated the exploration of other layered two-dimensional (2-D) materials beyond graphene.[1–4] In recent years, transition metal dichalcogenides (TMDs) have been the focal point of this research activity amongst which molybdenum disulphide (MoS_2) is the most studied material.[3,5–7] MoS_2 is a typical two-dimensional layered material with a honeycomb structure. A weak intra-layer van der Waals interaction enables its exfoliation down to a single stoichiometric unit (S-Mo-S) thick monolayer analogous to graphene.[8,9] Electronically, MoS_2 possesses an indirect band gap of ~1.3 eV in its bulk form, which transitions to a direct band gap of ~1.8 eV for the monolayer regime due to quantum confinement phenomena.[10,11] Furthermore, the absence of inversion symmetry in monolayer MoS_2 (as compared to the bulk material) gives rise to interesting applications like valleytronics and spintronics.[12,13] Thus, the reduction of the dimensions of MoS_2 opens up new avenues for a vast range of (opto-) electronic devices.[14–20] It has also been demonstrated that MoS_2 films in which the 2-D layers have out-of-plane orientations (with exposed edge sites) possess excellent electrocatalytic properties. The presence of dangling bonds and vacancies on the edge sites render these films highly catalytically active for the hydrogen evolution reaction in water splitting.[21–25] Therefore, MoS_2 has emerged as one of the frontrunner materials not only for future electronics,[12,13,26,27] but also as a potential alternative for precious noble metals in the area of electrocatalysis.[28–30] To capitalize on the extraordinary properties of MoS_2 there has been a quest for scalable, facile synthesis methods with ability to control both the thickness as well as the morphology. To date, most of these studies have focused on the synthesis of mono-to-few layers with in-plane orientation of the 2-D layers. A large variety of both top-down and bottom-up synthetic routes are reported in literature aiming at the synthesis of monolayer to few-layered MoS_2 thin films, for example, micro-mechanical and chemical exfoliation,[1,6,9,15,31–33] hydrothermal[34] and electrochemical methods,[35,36] physical vapor deposition,[37,38] chemical vapor deposition (CVD),[25,39–43] thermal vapor

[a]Department of Applied Physics, Eindhoven University of Technology, P.O. Box 513, 5600 MB Eindhoven, The Netherlands. E-mail: a.a.bol@tue.nl
[b]Philips Innovation Services, High Tech Campus 4, 5656 AE Eindhoven, The Netherlands
[c]Laboratory of Inorganic Materials Chemistry, Department Chemical Engineering and Chemistry, Eindhoven University of Technology, P.O. Box 513, 5600 MB Eindhoven, The Netherlands
[d]Oxford Instruments Plasma Technology, Yatton, BS49 4AP, UK

† Electronic supplementary information (ESI) available: Additional details about ALD saturation curves, XPS, Raman analysis, HRTEM, AFM, SEM and EIS. See DOI: 10.1039/c8nr02339e

sulphurization of Mo or MoO_3[44–46] *etc*. In contrast, despite the technological significance, there are only a few studies on controlling the film morphology, *i.e.* selective growth of out-of-plane oriented (OoPO) films. Most of these reports are based on high temperature techniques like CVD and rapid sulphurization of metal/metal oxide. For example, Li *et al.* have reported the synthesis of such OoPO nanostructures by using gas phase CVD at 750 °C.[23] Likewise, the rapid sulphurization of parent metal films (Mo films) at 550 °C–800 °C is also reported to yield out-of-plane growth of MoS_2 thin films.[22,47] Most of these techniques, however, provide insufficient control over thickness and tailoring of the morphology is not possible. Additionally, the requirement of a high processing temperature may hamper the development of this material on a technologically relevant scale. This paper discusses the use of atomic layer deposition (ALD) to deposit MoS_2 films with control over both thickness and morphology at a relatively low temperature (450 °C). ALD is a cyclic process based on self-limiting surface reactions which ensures Å-level thickness controllability and uniformity over large areas. The accurate thickness control offered by ALD has established it as a method of choice for high-k oxides in semiconductor industry.[48] Additionally, ALD offers a high conformality on intricate structures which are difficult to coat with any other gas phase technique. The application of ALD for 2-D materials is therefore of high interest and can be instrumental in the synthesis of high quality, large-area MoS_2. In literature, only a handful of reports on the synthesis of MoS_2 by means of ALD are available. Most of these studies have implemented either halide or carbonyl based metal precursors in combination with H_2S or CH_3SSCH_3 as co-reactant.[49–51] Some other groups have implemented Mo $(thd)_3$ and $Mo(NMe_2)_4$ as metal precursors in combination with H_2S.[52,53] These processes are shown to produce MoS_2 over a large area with a good control over thickness and thus exhibited the potential of ALD in 2-D world. However, most of these processes rely on high temperature post-annealing to improve the structural quality of the as-deposited 2-D films which is undesirable for industrial scalability (as discussed above) and remains an addressable issue.[50,54] Recently, anisotropic growth of 'edge-on' (OoPO) MoS_2 thin films by ALD using $MoCl_5$ in combination with H_2S has been reported.[55] However, the observed lateral inhomogeneity in growth rate over the wafer hints towards a possible CVD component in this process, which will disrupt the typical self-limiting ALD behavior and result in loss of precise thickness control.

In this work, we demonstrate that plasma enhanced ALD based on $[(NtBu)_2(NMe_2)_2Mo]$ and H_2S at 300 °C–450 °C is able to deliver archetypical precise thickness control and tuneable texture of the as-deposited MoS_2 films, while preserving the essence of ALD (*i.e.* self-limiting behaviour). We will first discuss the detailed investigation of the self-limiting behaviour, chemical composition of the as-deposited film and wafer-scale uniformity of the ALD process. Furthermore, the precise control over thickness from mono-layer to few layered regime is discussed. In the following sub-section, the influence of deposition temperature on the film morphology and crystallinity is presented. Next, the nucleation mechanism of MoS_2 thin films on SiO_2/Si substrates is elucidated and a model explaining the possible mechanism pertaining to the morphology transformation from in-plane to out-of-plane orientation for films deposited at 450 °C is also discussed. Finally, the control over film morphology is showcased by implementing the films with variant morphologies as electrocatalysts for the hydrogen evolution reaction (HER).

2. Experimental section

2.1 ALD process specifications

The MoS_2 thin films were deposited in an Oxford Instruments FlexAL™ ALD reactor[56,57] on 4″ Si wafers with a thermally grown 450 nm thick oxide layer on top. To maintain consistency throughout, all reported temperatures here refer to the set temperature of the substrate table which is called the 'growth temperature'. The Mo precursor employed was $[(NtBu)_2(NMe_2)_2Mo]$, (98%, Strem Chemicals) and was contained in a stainless steel canister which was heated to 50 °C. At this temperature, the vapor pressure of the precursor is reported to be 0.13 Torr.[58] The delivery lines were kept at 90 °C to avoid condensation of the precursor while the reactor walls were heated to 150 °C. For the precursor delivery to the deposition chamber a 100 sccm Ar (>99.999% purity) bubbling flow was employed. An intermediate Ar purge step with 100 sccm of Ar flow was applied after each precursor and plasma exposure steps. As the co-reactant, a H_2 + H_2S + Ar (8 sccm H_2; 2 sccm H_2S; 40 sccm Ar) plasma gas mixture generated in an inductively coupled plasma (ICP) source was used. The plasma power was 100 W with a reactor pressure of 6.6 mTorr during the plasma step. The ALD recipe was established with the first half cycle consisting of precursor dosing for 6 s followed by 6 s purge and 4 s pump down. The second half cycle used 20 s of plasma exposure with the same scheme for subsequent purge and pump as in the first half cycle. The film thickness evolution during deposition was monitored by *in situ* spectroscopy ellipsometry (J.A. Woollam M2000F, 1.25 eV–5 eV). The thickness values were extracted by employing the 'B-spline' model.

2.2 Film crystallinity and surface morphology

Grazing incidence X-ray diffraction (GI-XRD) was employed to determine the crystalline phases of the MoS_2 thin films. The XRD analysis was performed on a Panalytical X'Pert PRO MRD employing Cu Kα (1.54 Å) radiation with an incidence angle of 0.5° with respect to the substrate plane. Furthermore, Raman spectroscopy (RS) and photoluminescence (PL) spectroscopy measurements were performed with a Renishaw Raman microscope equipped with a 514 nm laser, integrated switchable gratings with 600 or 1800 lines per mm, and a CCD detector. For each scan, 5 accumulations with acquisition time of 10 s were taken. The surface morphology was studied by scanning electron microscopy (SEM) using a ZeissSigma Nanolab operating at an acceleration voltage of 2 kV. Additionally, atomic force microscopy (AFM) was also employed to study the surface

topology of the as-deposited films. The images were acquired at room temperature on Veeco dimension 3100 operated in tapping mode using Al coated Si tip (PointProbe Plus-NCHR) having a radius <7 nm. Images were processed in Gwyddion software with OpenGL interface and RMS roughness was obtained statistically from a scan area of 500 × 500 nm^2.

2.3 Chemical composition

To determine the elemental composition, X-ray photoelectron spectroscopy (XPS) was performed using a Thermo Scientific K-alpha spectrometer (Thermo Fisher Scientific, Waltham, MA) equipped with a monochromatic Al Kα X-ray radiation source ($h\nu$ = 1486.6 eV). For the XPS analysis, a 400 μm diameter spot was used and photoelectrons were collected at a take-off angle of 60°. The samples were neutralized during the XPS analysis using an electron flood gun in order to correct for differential or non-uniform charging. All peaks in the XPS survey scans are referenced to the binding energy of the C 1s peak of adventitious carbon (284.8 eV) for charge correction and quantification of the survey scans have been performed using Avantage software. Furthermore, Rutherford backscattering spectroscopy (RBS) was employed to determine the absolute chemical composition of the films. RBS was performed using a 1.523 MeV He + ion beam and a scatter angle of 170°.

2.4 Film microstructure

The film microstructure was determined by HRTEM analysis using a JEOL ARM 200F operated at 80 kV. For the top planar view images, MoS_2 films were grown on SiN_x TEM windows, coated with ~5 nm ALD SiO_2. Selected area electron diffraction (SAED) patterns were acquired from a 1.3 μm diameter area on each sample. For the cross-sectional imaging, the MoS_2 film was coated with a SiO_x film stack as a protective layer and subsequently prepared using a standard FIB lift-out TEM sample preparation scheme.

2.5 Electrochemical testing

MoS_2 films were deposited on glassy carbon plates polished by 0.3 μm Al_2O_3 slurry for electrochemical tests. The measurements were performed in a three electrode electrochemical workstation (Type: PGSTAT302N, Metrohm Autolab) with saturated calomel electrode (0.269 V *vs.* reversible hydrogen electrode (RHE) as a reference electrode, Pt foil (1 × 2 cm^2)) as a counter electrode and glassy carbon working electrode. All measurements were performed in 0.5 M H_2SO_4 electrolyte prepared using 18 MΩ cm deionized Milli-Q water purged with Ar for 20 min. Linear sweep voltammetry (LSV) experiments were conducted with a scan rate of 5 mV s^{-1} and AC electrochemical impedance spectroscopy was recorded at open circuit potential (OCP) in the frequency range of 10 kHz to 0.1 Hz. To calculate the Tafel slope, the linear portion at low overpotential region was fit to the Tafel equation using the internal resistance corrected LSV curves. Cyclic voltammetry (CV) stability tests were conducted with a scan rate of 50 mV s^{-1} starting at OCP from −0.52 V to 0.62 V.

3. Results and discussion

3.1 Characterization of the ALD process

3.1.1 Self-limiting growth, thickness control and uniformity. The self-limiting growth characteristics of the ALD process were investigated at a growth temperature of 250 °C. At this temperature, a saturated growth-per-cycle (GPC) of 0.1 nm per cycle is observed at the optimized precursor dose step and plasma exposure time of 6 s and 20 s, respectively. The saturation curves for the precursor dose step and plasma exposure time confirming the typical ALD behaviour are shown and further discussed in the ESI (Fig. S1†).

We measured the nominal film thickness as a function of number of cycles by *in situ* spectroscopic ellipsometry (SE). This was performed for ALD depositions over a large temperature range (150 °C–450 °C). The plot in Fig. 1(a) shows the evolution of film thickness as a function of number of ALD cycles for the entire investigated temperature range. Based on this plot, few observations can be made. Up to 300 °C, a linear relationship between film thickness and number of ALD cycles is observed, signifying the typical ALD behaviour. Above 350 °C, a non-linear increase in thickness is observed after 50 cycles, implying an increase in GPC during growth which is ascribed to a change in morphology by faster growth at the edge sites of MoS_2 as is discussed below. Also, it is worth mentioning that for all temperatures the film growth shows no nucleation delay during initial cycles, which is a highly valuable attribute for reproducible synthesis of mono-layer to thick MoS_2 films. Both from SE (Fig. 1(a)) and Rutherford backscattering spectroscopy (RBS) conducted for bulk regime *i.e.* film of 300 ALD cycles in each case (Fig. 1(b)), it is clear that the GPC increases with increasing temperature. This elevated growth rate at higher growth temperatures is most likely due to enhanced precursor adsorption owing to the formation of high surface area films with out-of-plane oriented (OoPO) morphology at higher growth temperatures. Additionally, it can also be speculated that the enhanced surface diffusion of metal atoms towards chemically more favourable edge sites (as compared to basal planes) of MoS_2 film deposited at higher growth temperature may contribute to the accelerated growth rate. The detailed discussion on the formation of OoPO films is provided later in this paper. To confirm that at 450 °C, the higher GPC is not a result of precursor decomposition in CVD – like reactions, a saturation study for the precursor half cycle was also performed at this temperature. The corresponding plot is shown in Fig. S1(d) (ESI†) which shows a plateau for the GPC with varying precursor dose and therefore ALD is confirmed at 450 °C precluding any role of precursor decomposition. The chemical composition of the as-deposited films was examined by X-ray photoelectron spectroscopy (XPS). The corresponding surface survey scan for the film deposited at 300 °C is shown in Fig. S2.1(a) (ESI†). This figure reveals that apart from characteristic Mo and S peaks, a small amount of O and C is also present on the film surface most probably due to atmospheric contamination. A high resolution X-ray photoelectron spectrum for the Mo 3d region (Fig. S2.1(b) in

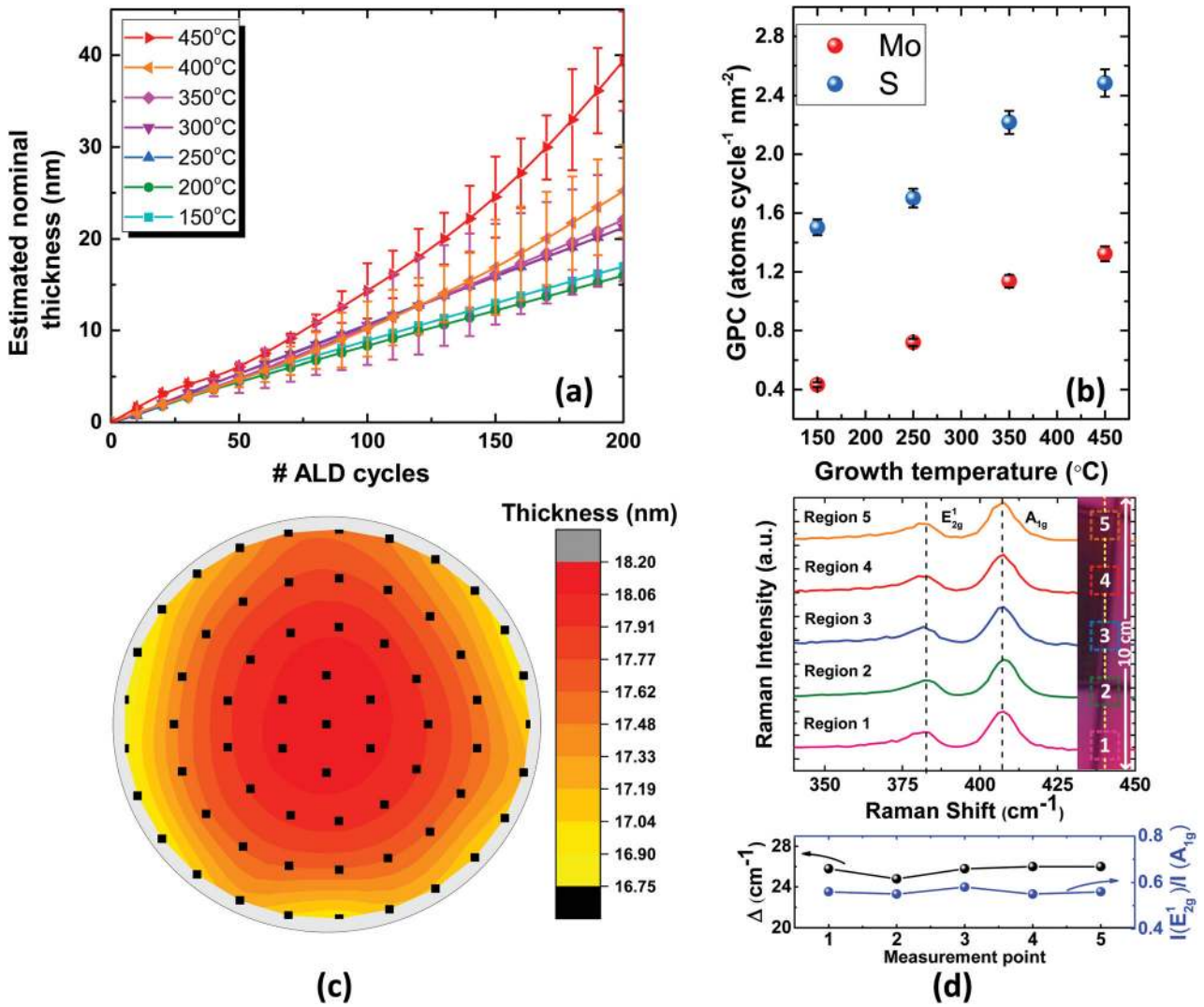

Fig. 1 (a) Layer thickness evolution as a function of number of ALD cycles over the whole investigated temperature range of 150 °C–450 °C. At higher growth temperatures, an increase in GPC can be seen. The error bars shown represent the sum of the measurement error, SE model fitting error and film roughness values. (b) RBS analysis showing a linear increase in individual GPC (atoms per cycle per nm^2) for both 'Mo' and 'S' with increasing growth temperatures. (c) Map of the thickness variation for film deposited at 300 °C (200 cycles) over a 4″ wafer carried out by *ex situ* SE showing a small thickness variation with a standard deviation of 0.4%. The black points on the wafer are the actual measurement points with 5 mm edge exclusion. (d) (top) Raman spectroscopy line scan (for the same wafer as in (c)) showing the five selective measurement points (step size ~2 cm) having consistent spectral features for a polycrystalline MoS_2 film registering a homogenous film over large area. (bottom) Plot showing the frequency difference (black) and relative Raman intensities (blue) for five measurement points.

ESI†) shows the doublet for MoS_2 (Mo^{4+}) with the 3d5/2 peak at 228.9 eV and the 3d3/2 peak at 232.1 eV which is in accordance with the binding energy positions given in the literature.[45,59,60]

Furthermore, a small fraction of Mo^{6+} is also detected corresponding to MoO_3 with binding energy position at 233.1 eV in line with the literature. The oxygen and carbon contaminants are only confined to the surface since a mild sputtering with Ar^+ ions results into almost complete removal of the two species with atomic % below the detection limit of XPS (Fig. S2.1(c, d) in ESI†). In addition, it was observed that the film composition is fairly stoichiometric in nature over the whole investigated growth temperature range. Table SI1 in the ESI† shows that the composition changes from slightly over-stoichiometric at low temperatures to under-stoichiometric at high temperatures, which has been frequently reported in the literature since the films produced by bottom-up synthesis methods can either be S-rich or possess S vacancies depending on the process parameters.

Subsequently, the film uniformity was analysed on a 4″ Si wafer as shown in Fig. 1(c). Spectroscopic ellipsometry (SE) was employed to measure the film thickness spatially across the wafer for a film deposited with 200 ALD cycles at a growth temperature of 300 °C. A small variation in film thickness is found over the scanned areas on the wafer (non-uniformity (% 1σ ((std. dev.)/(Avg.)) = 2.4)) clearly exhibiting a good thickness

uniformity. The uniformity of the grown film is a direct result of the typical self-limiting nature of an ALD process. A Raman line scan was also performed on the same 4″ wafer to study the uniformity in crystallinity of the as-deposited film. Fig. 1(d) shows the corresponding spectra with the signature vibrational peaks for crystalline MoS_2. The two characteristic Raman modes correspond to the in-plane (E^1_{2g}) and out-of-plane (A_{1g}) vibrational peak frequencies typically appearing at 382 cm^{-1} and 408 cm^{-1}, respectively.[61] In addition, the frequency difference between two modes (Δ) and relative Raman peak intensities as a function of measurement position are plotted as shown in Fig. 1(d). Very small variations in Δ: 24.8–26 cm^{-1} and in relative Raman peak intensity ($I(E^1_{2g})/I(A_{1g})$): 0.56–0.58, are found for the five measurements points, displaying a good uniformity over large area. Therefore, both SE and Raman analyses show that the synthesis of 2-D MoS_2 by our PEALD process is readily scalable.

3.1.2 Thickness control in the mono-to-few layer regime: Raman and PL analyses. Fig. 2(a) shows the control over film thickness in the initial phase of growth (first 50 ALD cycles) at 450 °C as measured by *in situ* SE analysis. However, in the mono layer to few layer regime, it is not easy to extract the exact thickness by SE, because of uncertainty in the optical properties of mono-to-few layer MoS_2.[62] Moreover, the change in surface termination groups (*e.g.* starting with –OH to possibly –SH) during subsequent ALD cycles might result into inaccurate thickness determination by SE analysis for a sub-nm thick film. This is the reason that despite the formation of a monolayer after 10 cycles (as will be shown below by Raman and PL analyses), the thickness extracted by SE modelling gives a value of ~1.3 nm than the expected ~0.6 nm for a monolayer of MoS_2.

Therefore, to validate the systematic control over thickness of ultra-thin MoS_2 films from monolayer to bulk by tuning the number of ALD cycles, the films deposited at 450 °C were also characterized by Raman and photoluminescence (PL) spectroscopy. Raman plots for the samples deposited using 10–50 ALD cycles are shown in Fig. 2(b). The two characteristic Raman peaks for MoS_2 corresponding to the vibrational modes (E^1_{2g} and A_{1g}) are observed for all the cases confirming continuous coverage with the 2H phase of MoS_2. The intensity and frequency difference between the two modes increases monotonically with the number of cycles as expected,[63] thus reflecting an excellent control over thickness with atomic scale precision. Importantly, the film after 10 cycles yields a frequency difference of ~20.6 cm^{-1} which is typically correlated with a monolayer of MoS_2.[39,64] The photoluminescence (PL) spectra are shown in Fig. 2(c). For 10 cycles, a strong peak at ~656 nm and a weak signal at ~612 nm are observed, which corresponds to the A and B excitonic peaks respectively and confirm the direct band gap in monolayer MoS_2.[11] The PL signal intensity is found to decrease as the film thickness increases with number of cycles. For MoS_2, this reduction in PL signal is generally attributed to a change in the electronic structure for thicker films (*i.e.* transition from direct to indirect band gap) which causes an increase in the intraband

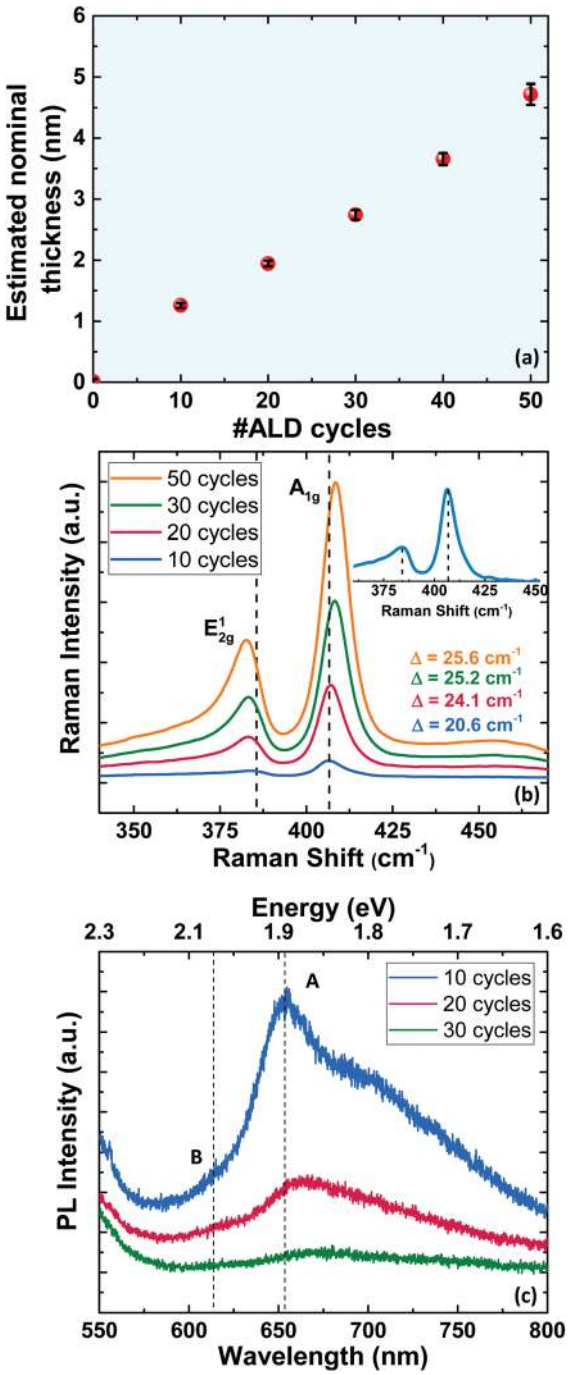

Fig. 2 (a) Thickness evolution of MoS_2 films in the initial phase of deposition at 450 °C as recorded by *in situ* SE analysis. (b) Raman evolution as a function of increasing number of cycles (at 450 °C) exhibiting excellent control over film thickness. The increasing frequency difference (Δ) between two vibrational modes with number of ALD cycles is an indicator for thickness increase. For clarity, the inset shows the enlarged Raman plot with two distinctive vibrational modes for a sample with 10 ALD cycles. The two vibrational modes are indicated by dotted lines. Also, the Raman peaks are normalized to the corresponding Si peak in each case. (c) The corresponding PL peak (λ_{ex} = 514 nm) for the thinnest film (10 cycles) is related to the direct band gap excitonic transition (positions for excitons A and B are highlighted with dotted lines) for a monolayer of MoS_2. The peak broadening is a clear indication of possible disorders present in the film.

relaxation rate from the excitonic states.[11] Thus, the presence of one MoS_2 monolayer after 10 ALD cycles is evidenced by both Raman and PL analyses. This is further corroborated by RBS analysis which shows that approximately ~13.2 Mo atoms per nm^2 are deposited after 10 cycles at 450 °C, which is very close to an ideal MoS_2 monolayer (approx. 11.6 Mo atoms per nm^2) for (001) plane.[65] A close inspection of Raman peaks reveals an asymmetric broadening for both vibrational modes which suggests the presence of structural disorder in the as-deposited films. This broadening is commonly observed for MoS_2 grown at low temperatures by bottom-up synthesis methods. We have used the Voigt fitting strategy based on the report from Mignuzzi *et al.*[66] to deconvolute the Raman spectrum for the film deposited after 10 cycles at 450 °C, and the corresponding plot is shown in Fig. S3(a) (ESI†). Apart from the two predominant vibrational peaks (*i.e.* E^1_{2g} and A_{1g}), three additional defect-induced peaks are observed that can be assigned to transverse optical (TO), longitudinal optical (LO) and out-of-plane optical (ZO) branches originating at the M point of the Brillouin zone.[63] Furthermore, in the low-frequency region of the Raman spectrum, a broad peak located at ~227 cm^{-1} is also observed (Fig. S3(b) in ESI†). This peak is attributed to the disorder induced LA(M) band and has been demonstrated as a metric for quantification of structural defects in MoS_2 by several groups.[43,63] Overall, the strong E^1_{2g} and A_{1g} modes combined with the low LA(M) peak shows that our process enables the deposition of good quality MoS_2 films at relatively low temperatures.

3.1.3 Control over film morphology. Tuning of the film morphology was achieved by modulating the growth temperature, providing an opportunity to adjust the density of active sites for eletrocatalytic applications. The effect of growth temperature on the morphology and crystallinity of the resulting film was initially examined by scanning electron microscopy (SEM) and Raman spectroscopy analyses, respectively. Top view SEM images and corresponding Raman spectra of films deposited in the temperature range 200 °C–450 °C (200 cycles each) are shown in Fig. 3(a–f). The film grown at 200 °C is found to be predominantly amorphous in nature with no characteristic Raman peaks except for the peak from the Si substrate (520 cm^{-1}). As the growth temperature is increased to 250 °C, a few nano-crystallites are recognizable in SEM. This small crystalline fraction yields very weak Raman signals due to the considerable contribution from the amorphous background. The characteristic Raman peaks for polycrystalline material become clear and distinct at a growth temperature of 300 °C where the density of crystallites is clearly higher, evidencing the poly-crystalline nature of the film. For growth temperatures from 350 °C to 450 °C, the crystallite size is larger and the film appears to become highly textured with

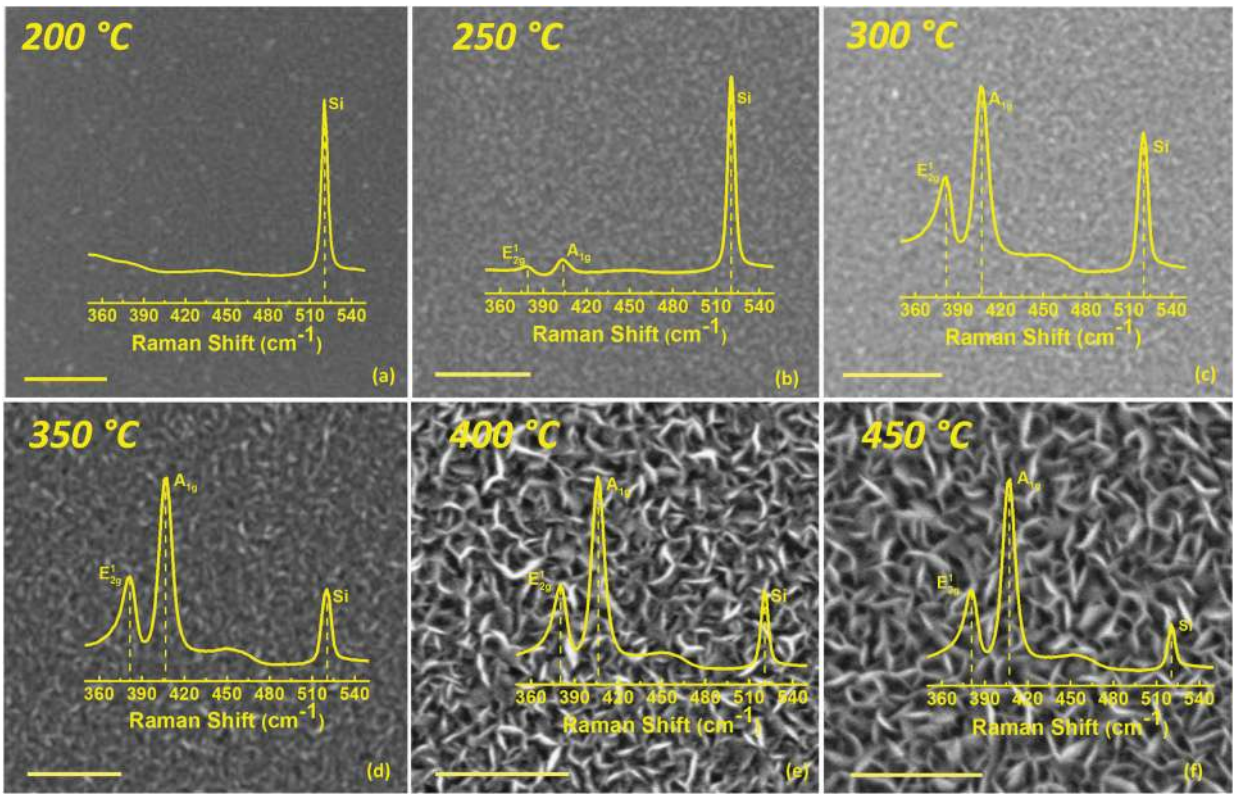

Fig. 3 (a–f) Top view SEM images (the scale bar in each image is 200 nm) showing the microstructure of the films grown at various growth temperatures for 200 cycles. The film morphology changes from amorphous to polycrystalline as the growth temperature increases from 200 °C to 450 °C. The overlying Raman spectra show the vibrational mode peaks evidencing an increase in the crystalline nature of the film at higher growth temperatures.

out-of-plane orientation (OoPO film). The corresponding Raman signal shows clear, distinctive vibrational peaks confirming the polycrystalline nature of the film. High-angle annular dark-field (HAADF) and high-resolution transmission electron microscopy images of a film grown at 450 °C (200 ALD cycles) are shown in Fig. S4(a & b in ESI†) where out-of-plane nanostructures uniformly distributed over the substrate are clearly observable. These nanostructures are found to be rough (root mean square roughness: 5.2 nm) in nature as evident in the AFM image (Fig. S4(c) in ESI†).

To complement SEM and Raman analysis, the influence of temperature on crystallinity and a possible preferred growth orientation of the films was analysed by X-ray diffraction (XRD) using two different detection geometries. First, grazing-incidence XRD (GI-XRD) studies were performed on samples grown for 200 cycles in the entire temperature range (200 °C–450 °C). GI-XRD is a technique well suited for analysing thin samples, because of the increased interaction volume as compared to a gonio (symmetric θ-2θ) scan. The GI X-ray diffractogram in Fig. 4(a) shows broad peaks at *ca.* 14.3° for growth temperatures of 200 °C and 250 °C. This peak corresponds to the (002) reflection of the semiconducting 2H phase of MoS_2.[67] However, the broad nature of the peaks at 200 °C and 250 °C indicates a predominant amorphous nature of the films at these temperatures as was already revealed by SEM and Raman analyses. At 300 °C, a clear (002) peak is present, which can be correlated to the increased density of nano-crystallites as observed in SEM images. Comparison with the powder diffraction spectrum displayed in Fig. 4(a) (top panel) indicates that this film has a clear <002> texture. For growth temperatures ≥350 °C, two additional peaks at 33.4° and 58.8° corresponding to the (100) and (110) reflections are detected, implying a change in texture.

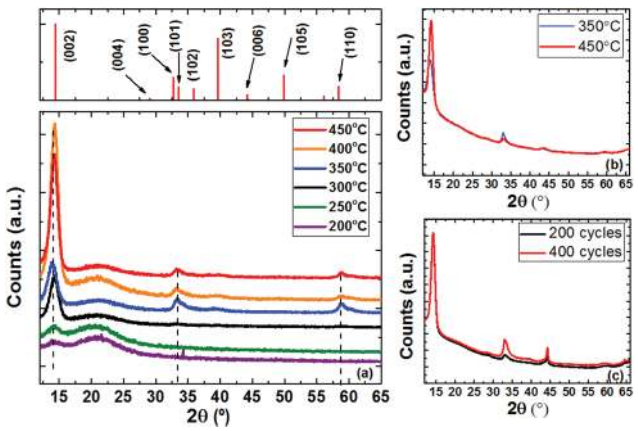

Fig. 4 (a) Grazing X-ray diffractograms of as-deposited MoS_2 films on SiO_2/Si substrates at various growth temperatures (200 cycles each). The position of peaks corresponding to (002), (100) and (110) is highlighted with dotted lines. The powder diffractogram for 2-H MoS_2 (JCPDF 037-1492) is shown as a reference for the reader (top panel). Gonio scans (symmetric θ–2θ) for (b) films deposited at 350 °C and 450 °C (200 cycles each) (c) films deposited with varying number of cycles at 450 °C.

To investigate this change in more detail, gonio scans were performed for a selection of samples. Fig. 4(b) shows diffractograms of samples deposited for 200 cycles at 350 °C and 450 °C. The change in relative peak heights implies an increase in <002> texture at higher temperatures. Note that there is a factor of 2 difference in layer thickness for these samples (see Fig. 1(a)). This also needs to be taken into account which is investigated in more detail by comparing the crystallographic orientation of the films deposited with 200 and 400 cycles at 450 °C. Fig. 4(c) demonstrates that the intensity of the (002) peak is identical for both samples, while the (100) and (110) peaks increase for higher number of ALD cycles. Here, it is essential to realize that the (100) and (110) planes are oriented orthogonal to the 2-D planes. This can be explained by a change in growth mode from in-plane growth for the lower part of the layer to out-of-plane growth for the later growth cycles. Comparison of Fig. 4(b) and (c) indicates that the transformation to OoPO growth occurs at an earlier stage (lower number of cycles) at lower temperatures.

3.1.4 Nucleation mechanism of PEALD of MoS_2 on SiO_2/Si. In order to improve control over the thickness and morphology of the MoS_2 formed by ALD, it is of key importance to understand the nucleation behaviour and appearance of out-of-plane growth mode of the MoS_2 on SiO_2. Generally, the crystal growth of MoS_2 begins with the nucleation of flat, crystal domains with in-plane orientation, as is reported in numerous bottom-up synthesis methods.[39,68] However, the film morphology transformation from the in-plane to out-of-plane mode is also reported. In literature, the out-of-plane growth of MoS_2 and graphene has been shown by using mainly high temperature CVD or metal/metal oxide sulphurization techniques. Several reasons responsible for such morphology are mentioned. For instance, Li *et al.* have shown that during CVD growth, the compression and extrusion between MoS_2 island layers ultimately leads to structural distortions resulting in out-of-plane standing MoS_2 nanosheets.[23] In another report by Kong *et al.*, it is argued that the rapid sulphurization of Mo films renders the perpendicular orientation to the MoS_2 films.[22] For growth of graphene by electron cyclotron resonance chemical vapor deposition (ECR-CVD),[69] the role of plasma species, causing localized hot spots and chemical potential gradients on the substrate, has been ascribed as one of the factors enhancing out-of-plane growth. Another conceivable factor which cannot be ruled out is stress development in the film, which upon relaxation may distort the basal plane oriented film morphology and promote out-of-plane growth.

In our PEALD process, most of the above mentioned factors can play a role for the morphology transformation. Therefore, to further elucidate the nucleation mechanism of MoS_2 on SiO_2/Si and gain deeper insight into the observed morphology transformation, HAADF-STEM analysis was performed on films grown at 450 °C at different stages of growth by varying the number of ALD cycles from 5 till 200. The corresponding images are shown in Fig. 5(a–f). A clear progression from nucleation of the film to the formation of OoPO films can be observed. A close inspection reveals that the film growth starts

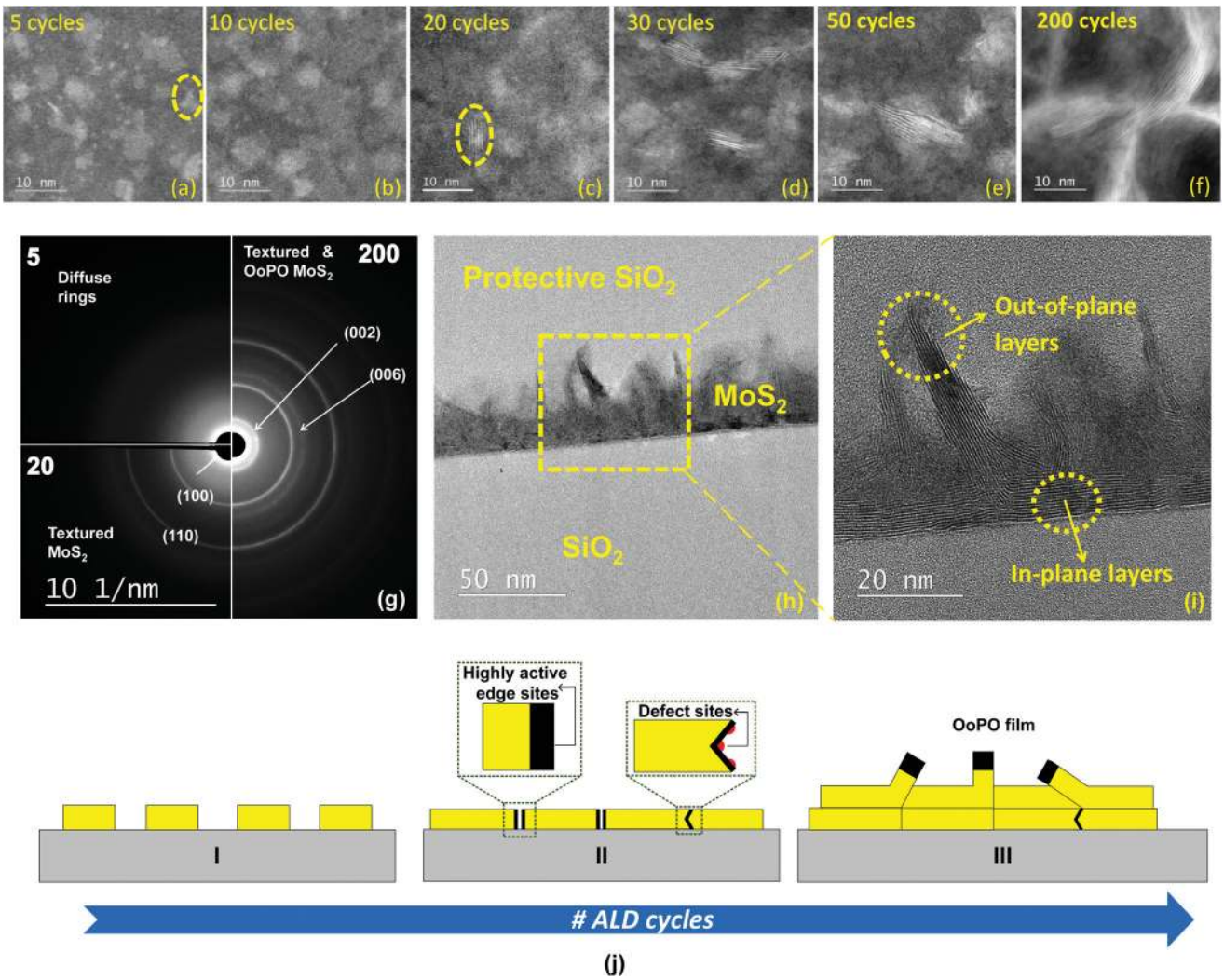

Fig. 5 (a–f) HAADF-STEM images showing the nucleation of MoS_2 on SiO_2/Si substrates as a function of number of ALD cycles and the variation of morphological structures. The in-plane flat, triangular domain and out-of-plane stripe-like patterns are highlighted by encircling (dashed line) in (a), (c) respectively. (g) The formation of textured and out-of-plane standing MoS_2 nanostructures is supported by the electron diffraction patterns showing bright rings corresponding to (002) and (006) crystal orientations. The diffraction patterns are labelled with the corresponding number of ALD cycles (5, 20, 200) accordingly. (h) Cross sectional TEM image of a MoS_2 thin film deposited at 450 °C (200 cycles) on SiO_2/Si substrate with a top SiO_2 layer deposited for protection during sample preparation. (i) The magnified view reveals the transformation from in-plane growth to out-of-plane standing structures. (j) Schematic showing the growth model for the development of OoPO nanostructures with random orientations.

with the formation of discrete flat MoS_2 islands which appear as triangular or star shaped domains as highlighted in Fig. 5(a). The formation of such flat triangular or star shaped domains with in-plane orientation is typical for synthesis of MoS_2 *via* bottom up techniques as mentioned earlier.

After 10 ALD cycles, these discrete islands are found to extend in the lateral direction and merge at certain points to form an almost continuous film. Some bi- to few-layer fragments can be observed as well. Thereafter, in case of 20 cycles, the emergence of stripe-like patterns representing nano-scale out-of-plane nanostructures, can be observed which have been highlighted in Fig. 5(c). This suggests that the transformation from in-plane to out-of-plane plane growth mode is thickness dependent and takes place after a closed film of horizontally oriented domains is formed. The size and density of these out-of-plane nanostructures is found to increase with increasing number of ALD cycles. At 200 cycles, the out-of-plane growth mode is clearly dominating as shown Fig. 5(f). Fig. 5(g) shows the corresponding selective area electron diffraction (SAED) patterns for films grown with increasing number of cycles. It can be observed that the film after 5 cycles has weak, diffuse diffraction rings as can be expected because of the limited size of the islands.

In case of 20 cycles, a set of sharp diffraction rings is present, characteristic for a polycrystalline film with small grain sizes. In the present case of SAED under normal incidence of the electron beam on the sample, the vertically oriented crystallographic planes are visualized in the SAED

pattern. The absence of (002) and (006) rings and the presence of the closed (100) and (110) rings indicates the presence of a <001> texture within in-plane rotational freedom of the domains.

For a higher number of cycles (200 cycles), the intensity of the rings increases as more volume is probed. In addition, (002) and (006) orientations are clearly visible, representing the out-of-plane orientation of the 2-D planes, in agreement with the observation of nanostructures for this sample.

To further elucidate the morphology of the OoPO growth mode, cross-sectional TEM analysis was carried out on a thick MoS_2 film as depicted in Fig. 5(h). The magnified image in Fig. 5(i) clearly shows the two types of morphologies: 2-D layers parallel to the substrate surface close to the interface and emergence of OoPO nanostructures which seem to start out from a large variation in orientations but are driven out-of-plane due to crowding with increasing film thickness. A close look reveals that the transformation from in-plane to out-of-plane growth mode occurs most likely at the grain boundaries. The final resulting film therefore comprises of a mixed morphology as shown earlier (Fig. S4 in ESI†). The in-plane orientation of the first few layers points towards the negligible role of the substrate on the out-of-plane growth mode. To prove this hypothesis, we considered various substrates (ALD grown Al_2O_3, Au coated Si, exfoliated MoS_2 flakes, Glassy carbon) and carried out similar depositions under identical conditions. The resulting film morphology (*i.e.* OoPO) was consistent irrespective of the substrate used including the mechanically exfoliated MoS_2 flakes. This indicates that the development of the OoPO growth mode is independent of the substrate used and is rather related to the growth mechanism for this material. The corresponding top view SEM images are shown in Fig. S5 (ESI†).

Based on these results, a growth model is postulated and schematically illustrated in Fig. 5(j). In this model, it is shown that the film growth starts with the formation of islands with horizontal basal plane orientation on the substrate. The growth at the edges of these islands is faster than growth on top of the basal planes. This can be ascribed to the fact that the edge of a 2-D layer consist of dangling bonds, which act as preferable sites for precursor adsorption, unlike the inert basal planes. Adding a new 2-D layer on top of the basal plane implies nucleation of a new layer, which is energetically less favourable than lateral growth of already existing planes. Next, when the discrete islands coalesce, defect sites at the grain boundaries might occur due to the different in-plane orientations of the individual crystals (as concluded from SAED). These defect sites can act as new active sites for precursor adsorption, from which new MoS_2 crystals form. However, due to crowding effects these new crystals do not necessarily grow in-plane, but have random out-of-plane orientation as observed above.

Overall, the morphology transformation can be a result of a complex interplay of different factors. To sum up, we hypothesize an additional possible governing mechanism *i.e.* the enhanced adsorption of precursor on the edge and defect sites during ALD growth ultimately giving rise to out-of-plane growth mode.

3.2 Hydrogen evolution reaction (HER) performance

Electrolytic water splitting is one of the most efficient and sustainable ways to produce hydrogen from water.[70] Out-of-plane oriented transition metal dichalcogenides (TMDs) thin films with catalytically active edge sites synthesized by various bottom-up methods have emerged as an inexpensive alternative to the precious noble metals (*e.g.* Pt) for HER.[21,71] ALD provides an excellent opportunity to modulate the thickness and height of the out-of-plane oriented films which can be a great advantage over other bottom-up synthesis techniques. In past, several groups have demonstrated the HER performance of ALD synthesized amorphous and polycrystalline MoS_2 films.[72,73] However, the poor stability of amorphous films and requirement of post annealing calls for further investigation of ALD synthesized MoS_2 films for HER mechanism. In this work, we therefore focus on assessment of the HER performance of as-deposited polycrystalline films with different morphologies which can be easily modulated by using our PEALD process and might be a valuable asset for electrocatalysis applications.

Glassy carbon (GC) plates were chosen as substrates since they are conductive, chemically stable, electrochemically inert in a large potential window and can be polished to a mirror finish. These substrates were subjected to an increasing number of ALD cycles (10–600 cycles) at 450 °C under optimum conditions. While a flat film was obtained after 10 cycles (as shown previously), for 100, 400 and 600 cycles, OoPO films of different thicknesses were obtained. Fig. 6(a) shows the cathodic polarization curves for MoS_2 films and a bare GC substrate as reference. It is clearly observed that all MoS_2 coated samples possess a much lower onset overpotential (η) for HER than the bare GC substrate. Notably, the sample with 10 ALD cycles shows a substantial catalytic activity which suggests the presence of active edge sites in the early growth stages of the film. This confirms the TEM observation that for 10 ALD cycles the layer is not completely closed yet and edges of 2-D islands are exposed. The samples possessing OoPO films (100, 400 and 600 cycles) have higher cathodic current densities (at η = 500 mV). This indicates an enhanced HER performance owing to an increased number of active edge sites of the OoPO nanostructures.

Table 1 summarizes the figures of merit for all investigated samples. Generally, the overpotential required to drive a cathodic current density of 10 mA cm^{-2} (η_{10}) is used as a figure of merit for the overall performance of electrocatalysts.[74] It is to be noted that the value of η_{10} reduces with an increase in ALD cycles from 10 to 100 most likely due to morphology transformation implying an increase in the number of edge sites causing a higher HER performance. However, the further increment in number of ALD cycles (from 100 till 600) does not show a considerable improvement in HER performance which is attributed to the saturation of active surface area as reflected in double layer capacitance measurements shown in Fig. S6(a) (ESI†). It should be noted that the double layer capacitance value for the sample with 10 cycles is overestimated, because of the high surface roughness (RMS 3.6 nm) of

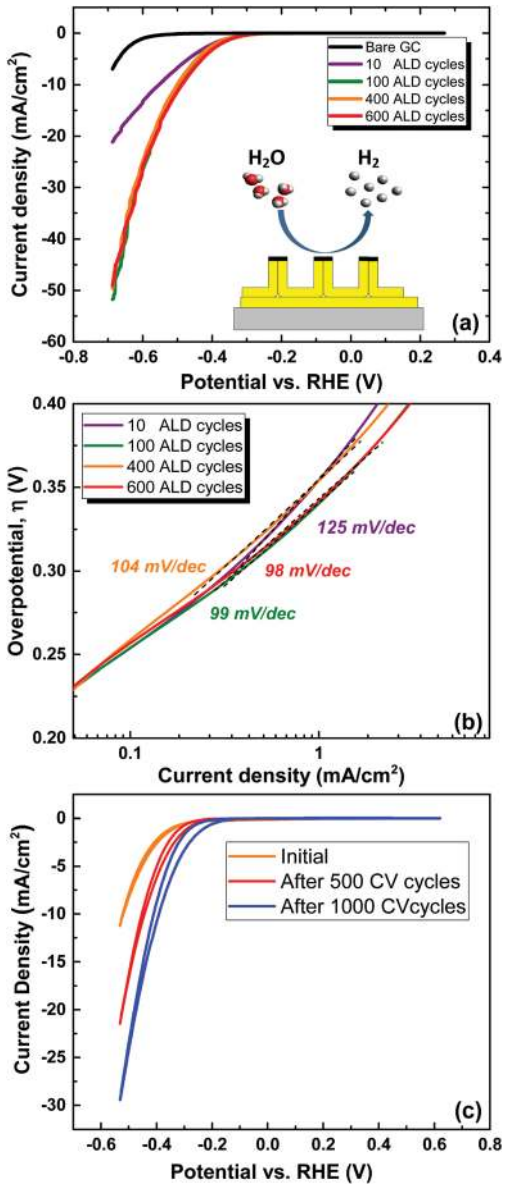

Fig. 6 (a) HER polarization curve (linear sweep voltammetry) for OoPO MoS_2 films deposited on GC substrate showing an onset overpotential of around −0.26 V. In the inset, a cartoon is shown where the hydrogen evolution by splitting of water molecule assisted by OoPO films is depicted. (b) Tafel plot showing the calculated Tafel slopes for all the investigated samples. (c) Cyclic voltammetry repeated for 1000 cycles showing an improved activity for the as-deposited OoPO MoS_2 film (400 ALD cycles).

Table 1 Key parameters extracted from the electrochemical characterization of different samples with varying number of PEALD cycles

Sample	Tafel slope (mV per decade)	η_{10} (mV)
10 cycles	125	−553
100 cycles	99	−487
400 cycles	104	−503
600 cycles	98	−488

the polished GC substrate as shown in the inset of Fig. S6(a).† Furthermore, the corresponding Tafel plots are shown in Fig. 6(b) revealing Tafel slopes for the investigated samples in the range of 98–125 mV per dec.

In literature, the value of Tafel slope for MoS_2 based catalysts has shown a large spread ranging from 40 to 220 mV per dec depending on the material preparation and modification methods.[75] It is worth mentioning that the HER performance of our OoPO MoS_2 films (Tafel slopes: 98–125 mV per decade and exchange current density values: 1.8–1.9 μA cm^{-2}) is comparable to the films with similar morphology (*viz.* vertically aligned, edge enriched MoS_2 thin film *etc.*) prepared by other techniques as reported in the literature.[22,75] The stability of as-deposited OoPO MoS_2 films was assessed by taking continuous cyclic voltammograms (CV). The corresponding CV curves before and after 1000 cycles are shown in Fig. 6(c). Interestingly, the performance is improved after 1000 cycles of continuous CV test which can be attributed to the formation of sulphur vacancies during HER. It is well known that the introduction of sulphur vacancies may result in higher reactivity owing to the generation of additional catalytic sites.[76,77]

It is important to mention that all samples subjected to HER tests have been used as-deposited and therefore further optimization of the overall HER performance should be possible and follow-up work will be done accordingly. Yet, these results confirm the viability of the PEALD process to modulate the film morphology and thickness of out-of-plane nanostructures for efficient utilization in electrocatalysis. The large area growth and low temperature processing possible by PEALD are the other virtues which can be highly advantageous for eletrocatalytic applications.

4. Conclusions

In summary, we report on a large-scale, low temperature PEALD process for synthesizing uniform, high quality 2-D MoS_2 films. Our process shows precise thickness control down to a monolayer and provides possibilities to tune the morphology of the layers by varying the growth temperature from 150–450 °C. Extensive film characterization has helped in understanding the influence of growth temperature on film morphology, crystallinity and chemical composition. Moreover, based on the detailed TEM investigation, we have proposed that during ALD growth, the enhanced precursor adsorption on the highly energetic edge sites of MoS_2 may play a role in the transformation to out-of-plane oriented films at 450 °C. Furthermore, the excellent control over morphology is showcased in electrocatalysis using the hydrogen evolution reaction (HER) in which the out-of-plane oriented films outperform flat, in-plane oriented films. These results show that ALD might be instrumental in realizing not only the uniform large area growth of high-quality 2-D materials but can also be applied as a tool to control the morphology of thin films which might result into interesting structures (including heterostructures) for multiple applications.

Conflicts of interest

There are no conflicts of interest to declare.

Acknowledgements

The authors would like to thank J. van Gerwen and C. A. A. van Helvoirt for technical assistance and N. F. W. Thissen for fruitful discussions. A. Omahony from Oxford Instruments is acknowledged for carrying out the thickness uniformity measurements. This work was financially supported by NWO and the Technology Foundation STW through the VIDI program on 'Novel bottom-up nanofabrication techniques for future carbon-nanoelectronics'. Dr B. Barcones is acknowledged for the FIB preparation of the TEM samples. Solliance and the Dutch province of Noord-Brabant are acknowledged for funding the TEM facility. L. W. and J. P. H. appreciate funding *via* the program "CO_2-neutral fuels" (project 13-CO26) of the late Foundation for Fundamental Research on Matter (FOM), financially supported by the Netherlands Organization for Scientific Research (NWO) and co-financed by Shell Global Solutions International B.V.

References

1 K. S. Novoselov, D. Jiang, F. Schedin, T. J. Booth, V. V. Khotkevich, S. V. Morozov and A. K. Geim, Two-dimensional atomic crystals, *Proc. Natl. Acad. Sci. U. S. A.*, 2005, **102**(30), 10451–10453.

2 M. Xu, T. Liang, M. Shi and H. Chen, Graphene-Like Two-Dimensional Materials, *Chem. Rev.*, 2013, **113**(5), 3766–3798.

3 X. Huang, Z. Zeng and H. Zhang, Metal dichalcogenide nanosheets: preparation, properties and applications, *Chem. Soc. Rev.*, 2013, **42**(5), 1934–1946.

4 H. Zhang, Ultrathin Two-Dimensional Nanomaterials, *ACS Nano*, 2015, **9**(10), 9451–9469.

5 K. Kang, S. Xie, L. Huang, Y. Han, P. Y. Huang, K. F. Mak, C.-J. Kim, D. Muller and J. Park, High-mobility three-atom-thick semiconducting films with wafer-scale homogeneity, *Nature*, 2015, **520**(7549), 656–660.

6 M. Chhowalla, H. S. Shin, G. Eda, L.-J. Li, K. P. Loh and H. Zhang, The chemistry of two-dimensional layered transition metal dichalcogenide nanosheets, *Nat. Chem.*, 2013, **5**(4), 263–275.

7 R. Ganatra and Q. Zhang, Few-Layer MoS_2: A Promising Layered Semiconductor, *ACS Nano*, 2014, **8**(5), 4074–4099.

8 P. Joensen, R. F. Frindt and S. R. Morrison, Single-layer MoS_2, *Mater. Res. Bull.*, 1986, **21**(4), 457–461.

9 G. Eda, H. Yamaguchi, D. Voiry, T. Fujita, M. Chen and M. Chhowalla, Photoluminescence from Chemically Exfoliated MoS_2, *Nano Lett.*, 2011, **11**(12), 5111–5116.

10 K. F. Mak, C. Lee, J. Hone, J. Shan and T. F. Heinz, Atomically Thin MoS_2: A New Direct-Gap Semiconductor, *Phys. Rev. Lett.*, 2010, **105**(13), 136805.

11 A. Splendiani, L. Sun, Y. Zhang, T. Li, J. Kim, C.-Y. Chim, G. Galli and F. Wang, Emerging Photoluminescence in Monolayer MoS_2, *Nano Lett.*, 2010, **10**(4), 1271–1275.

12 R. Suzuki, M. Sakano, Y. J. Zhang, R. Akashi, D. Morikawa, A. Harasawa, K. Yaji, K. Kuroda, K. Miyamoto, T. Okuda, K. Ishizaka, R. Arita and Y. Iwasa, Valley-dependent spin polarization in bulk MoS2 with broken inversion symmetry, *Nat. Nanotechnol.*, 2014, **9**(8), 611–617.

13 K. F. Mak, K. He, J. Shan and T. F. Heinz, Control of valley polarization in monolayer MoS_2 by optical helicity, *Nat. Nanotechnol.*, 2012, **7**(8), 494–498.

14 Q. H. Wang, K. Kalantar-Zadeh, A. Kis, J. N. Coleman and M. S. Strano, Electronics and optoelectronics of two-dimensional transition metal dichalcogenides, *Nat. Nanotechnol.*, 2012, **7**(11), 699–712.

15 B. Radisavljevic, A. Radenovic and J. Brivio, Single-layer MoS_2 transistors, *Nat. Nanotechnol.*, 2011, **6**, 147–150.

16 B. Radisavljevic, M. B. Whitwick and A. Kis, Integrated Circuits and Logic Operations Based on Single-Layer MoS_2, *ACS Nano*, 2011, **5**(12), 9934–9938.

17 Z. Yin, H. Li, H. Li, L. Jiang, Y. Shi, Y. Sun, G. Lu, Q. Zhang, X. Chen and H. Zhang, Single-Layer MoS_2 Phototransistors, *ACS Nano*, 2012, **6**(1), 74–80.

18 O. Lopez-Sanchez, D. Lembke, M. Kayci, A. Radenovic and A. Kis, Ultrasensitive photodetectors based on monolayer MoS_2, *Nat. Nanotechnol.*, 2013, **8**(7), 497–501.

19 K. F. Mak and J. Shan, Photonics and optoelectronics of 2D semiconductor transition metal dichalcogenides, *Nat. Photonics*, 2016, **10**(4), 216–226.

20 R. S. Sundaram, M. Engel, A. Lombardo, R. Krupke, A. C. Ferrari, P. Avouris and M. Steiner, Electroluminescence in Single Layer MoS_2, *Nano Lett.*, 2013, **13**(4), 1416–1421.

21 H. Wang, Z. Lu, S. Xu, D. Kong, J. J. Cha, G. Zheng, P.-C. Hsu, K. Yan, D. Bradshaw, F. B. Prinz and Y. Cui, Electrochemical tuning of vertically aligned MoS_2 nanofilms and its application in improving hydrogen evolution reaction, *Proc. Natl. Acad. Sci. U. S. A.*, 2013, **110**(49), 19701–19706.

22 D. Kong, H. Wang, J. J. Cha, M. Pasta, K. J. Koski, J. Yao and Y. Cui, Synthesis of MoS_2 and $MoSe_2$ Films with Vertically Aligned Layers, *Nano Lett.*, 2013, **13**(3), 1341–1347.

23 H. Li, H. Wu, S. Yuan and H. Qian, Synthesis and characterization of vertically standing MoS_2 nanosheets, *Sci. Rep.*, 2016, **6**, 21171.

24 F. Lan, Z. Lai, Y. Xu, H. Cheng, Z. Wang, C. Qi, J. Chen and S. Zhang, Synthesis of Vertically Standing MoS_2 Triangles on SiC, *Sci. Rep.*, 2016, **6**, 31980.

25 A. K. Min, K. K. Seong, H. Jin Kyu, K. Seong Jun, C. Sung-Jin, P. Chong-Yun, M. Sung, S. Wooseok, L. Sun Sook, L. Jongsun and A. Ki-Seok, Large scale growth of vertically standing MoS_2 flakes on 2D nanosheet using organic promoter, *2D Mater.*, 2017, **4**(2), 025042.

26 S. B. Desai, S. R. Madhvapathy, A. B. Sachid, J. P. Llinas, Q. Wang, G. H. Ahn, G. Pitner, M. J. Kim, J. Bokor, C. Hu,

H.-S. P. Wong and A. Javey, MoS_2 transistors with 1-nanometer gate lengths, *Science*, 2016, **354**(6308), 99–102.

27 L. Kai-Shin, W. Bo-Wei, L. Lain-Jong, L. Ming-Yang, C. Chia-Chin Kevin, H. Cho-Lun, L. Chang-Hsien, C. Yi-Ju, C. Chun-Chi, W. Chien-Ting, C. Min-Cheng, S. Jia-Min, Y. Wen-Kuan, C. Yu-Lun, Y. Fu-Liang and H. Chenming, In MoS_2 U-shape MOSFET with 10 nm channel length and poly-Si source/drain serving as seed for full wafer CVD MoS_2 availability, *IEEE Symposium on VLSI Technology, 14–16 June 2016*, 2016, pp. 1–2.

28 R. R. Chianelli, Fundamental Studies of Transition Metal Sulfide Hydrodesulfurization Catalysts, *Catal. Rev.*, 1984, **26**(3–4), 361–393.

29 D. Merki and X. Hu, Recent developments of molybdenum and tungsten sulfides as hydrogen evolution catalysts, *Energy Environ. Sci.*, 2011, **4**(10), 3878–3888.

30 F. Wang, T. A. Shifa, X. Zhan, Y. Huang, K. Liu, Z. Cheng, C. Jiang and J. He, Recent advances in transition-metal dichalcogenide based nanomaterials for water splitting, *Nanoscale*, 2015, **7**(47), 19764–19788.

31 J. N. Coleman, M. Lotya, A. O'Neill, S. D. Bergin, P. J. King, U. Khan, K. Young, A. Gaucher, S. De, R. J. Smith, I. V. Shvets, S. K. Arora, G. Stanton, H.-Y. Kim, K. Lee, G. T. Kim, G. S. Duesberg, T. Hallam, J. J. Boland, J. J. Wang, J. F. Donegan, J. C. Grunlan, G. Moriarty, A. Shmeliov, R. J. Nicholls, J. M. Perkins, E. M. Grieveson, K. Theuwissen, D. W. McComb, P. D. Nellist and V. Nicolosi, Two-Dimensional Nanosheets Produced by Liquid Exfoliation of Layered Materials, *Science*, 2011, **331**(6017), 568–571.

32 A. Y. S. Eng, A. Ambrosi, Z. Sofer, P. Šimek and M. Pumera, Electrochemistry of Transition Metal Dichalcogenides: Strong Dependence on the Metal-to-Chalcogen Composition and Exfoliation Method, *ACS Nano*, 2014, **8**(12), 12185–12198.

33 Y. Yao, Z. Lin, Z. Li, X. Song, K.-S. Moon and C.-p. Wong, Large-scale production of two-dimensional nanosheets, *J. Mater. Chem.*, 2012, **22**(27), 13494–13499.

34 P. Yiya, M. Zhaoyu, Z. Chang, L. Jun, Y. Weichao, J. YunBo and Q. Yitai, Hydrothermal Synthesis and Characterization of Single-Molecular-Layer MoS_2 and $MoSe_2$, *Chem. Lett.*, 2001, **30**(8), 772–773.

35 T. Stephenson, Z. Li, B. Olsen and D. Mitlin, Lithium ion battery applications of molybdenum disulfide (MoS_2) nanocomposites, *Energy Environ. Sci.*, 2014, **7**(1), 209–231.

36 P. K. Kannan, D. J. Late, H. Morgan and C. S. Rout, Recent developments in 2D layered inorganic nanomaterials for sensing, *Nanoscale*, 2015, **7**(32), 13293–13312.

37 J. Tao, J. Chai, X. Lu, L. M. Wong, T. I. Wong, J. Pan, Q. Xiong, D. Chi and S. Wang, Growth of wafer-scale MoS_2 monolayer by magnetron sputtering, *Nanoscale*, 2015, **7**(6), 2497–2503.

38 H. Jyun-Hong, C. Hsing-Hung, L. Pang-Shiuan, L. Li-Syuan, W. Chien-Ting, C. Cheng-Tung, L. Yao-Jen, L. Lain-Jong, C. Wen-Hao and H. Tuo-Hung, Large-area few-layer MoS_2 deposited by sputtering, *Mater. Res. Express*, 2016, **3**(6), 065007.

39 S. Najmaei, Z. Liu, W. Zhou, X. Zou, G. Shi, S. Lei, B. I. Yakobson, J.-C. Idrobo, P. M. Ajayan and J. Lou, Vapour phase growth and grain boundary structure of molybdenum disulphide atomic layers, *Nat. Mater.*, 2013, **12**(8), 754–759.

40 A. M. van der Zande, P. Y. Huang, D. A. Chenet, T. C. Berkelbach, Y. You, G.-H. Lee, T. F. Heinz, D. R. Reichman, D. A. Muller and J. C. Hone, Grains and grain boundaries in highly crystalline monolayer molybdenum disulphide, *Nat. Mater.*, 2013, **12**(6), 554–561.

41 J. Chen, W. Tang, B. Tian, B. Liu, X. Zhao, Y. Liu, T. Ren, W. Liu, D. Geng, H. Y. Jeong, H. S. Shin, W. Zhou and K. P. Loh, Chemical Vapor Deposition of High-Quality Large-Sized MoS_2 Crystals on Silicon Dioxide Substrates, *Adv. Sci.*, 2016, **3**(8), 1600033.

42 X. Ling, Y.-H. Lee, Y. Lin, W. Fang, L. Yu, M. S. Dresselhaus and J. Kong, Role of the Seeding Promoter in MoS_2 Growth by Chemical Vapor Deposition, *Nano Lett.*, 2014, **14**(2), 464–472.

43 M. Elisha, G. Andy, M. Jonathan, C. Mike and S. S. Ravi, A Raman metrology approach to quality control of 2D MoS_2 film fabrication, *J. Phys. D: Appl. Phys.*, 2017, **50**(18), 184005.

44 Y. C. Lin, W. Zhang, J. K. Huang, K. K. Liu, Y. H. Lee and C. T. Liang, Wafer-scale MoS_2 thin layers prepared by MoO_3 sulfurization, *Nanoscale*, 2012, **4**, 6637–6641.

45 Y. Zhan, Z. Liu, S. Najmaei, P. M. Ajayan and J. Lou, Large-Area Vapor-Phase Growth and Characterization of MoS_2 Atomic Layers on a SiO_2 Substrate, *Small*, 2012, **8**(7), 966–971.

46 N. Choudhary, J. Park, J. Y. Hwang and W. Choi, Growth of Large-Scale and Thickness-Modulated MoS_2 Nanosheets, *ACS Appl. Mater. Interfaces*, 2014, **6**(23), 21215–21222.

47 Y. Jung, J. Shen, Y. Liu, J. M. Woods, Y. Sun and J. J. Cha, Metal Seed Layer Thickness-Induced Transition From Vertical to Horizontal Growth of MoS_2 and WS_2, *Nano Lett.*, 2014, **14**(12), 6842–6849.

48 K. Mistry, C. Allen, C. Auth, B. Beattie, D. Bergstrom, M. Bost, M. Brazier, M. Buehler, A. Cappellani, R. Chau, C. H. Choi, G. Ding, K. Fischer, T. Ghani, R. Grover, W. Han, D. Hanken, M. Hattendorf, J. He, J. Hicks, R. Huessner, D. Ingerly, P. Jain, R. James, L. Jong, S. Joshi, C. Kenyon, K. Kuhn, K. Lee, H. Liu, J. Maiz, B. McIntyre, P. Moon, J. Neirynck, S. Pae, C. Parker, D. Parsons, C. Prasad, L. Pipes, M. Prince, P. Ranade, T. Reynolds, J. Sandford, L. Shifren, J. Sebastian, J. Seiple, D. Simon, S. Sivakumar, P. Smith, C. Thomas, T. Troeger, P. Vandervoorn, S. Williams and K. Zawadzki, In A 45nm Logic Technology with High-k + Metal Gate Transistors, Strained Silicon, 9 Cu Interconnect Layers, 193nm Dry Patterning, and 100% Pb-free Packaging, *2007 IEEE International Electron Devices Meeting, 10–12 Dec. 2007*, 2007, pp. 247–250.

49 L. K. Tan, B. Liu, J. H. Teng, S. Guo, H. Y. Low and K. P. Loh, Atomic layer deposition of a MoS_2 film, *Nanoscale*, 2014, **6**(18), 10584–10588.

50 Z. Jin, S. Shin, D. H. Kwon, S.-J. Han and Y.-S. Min, Novel chemical route for atomic layer deposition of MoS_2 thin

film on SiO_2/Si substrate, *Nanoscale*, 2014, **6**(23), 14453–14458.

51 A. Valdivia, D. J. Tweet and J. F. Conley Jr., Atomic layer deposition of two dimensional MoS_2 on 150 mm substrates, *J. Vac. Sci. Technol., A*, 2016, **34**(2), 1–5.

52 M. Mattinen, T. Hatanpää, T. Sarnet, K. Mizohata, K. Meinander, P. J. King, L. Khriachtchev, J. Räisänen, M. Ritala and M. Leskelä, Atomic Layer Deposition of Crystalline MoS_2 Thin Films: New Molybdenum Precursor for Low-Temperature Film Growth, *Adv. Mater. Interfaces*, 2017, 1700123.

53 T. Jurca, M. J. Moody, A. Henning, J. D. Emery, B. Wang, J. M. Tan, T. L. Lohr, L. J. Lauhon and T. J. Marks, Low-Temperature Atomic Layer Deposition of MoS_2 Films, *Angew. Chem., Int. Ed.*, 2017, **56**(18), 4991–4995.

54 J. J. Pyeon, S. H. Kim, D. S. Jeong, S.-H. Baek, C.-Y. Kang, J.-S. Kim and S. K. Kim, Wafer-scale growth of MoS_2 thin films by atomic layer deposition, *Nanoscale*, 2016, **8**(20), 10792–10798.

55 T. A. Ho, C. Bae, S. Lee, M. Kim, J. M. Montero-Moreno, J. H. Park and H. Shin, Edge-On MoS_2 Thin Films by Atomic Layer Deposition for Understanding the Interplay between the Active Area and Hydrogen Evolution Reaction, *Chem. Mater.*, 2017, **29**(17), 7604–7614.

56 S. B. S. Heil, J. L. van Hemmen, C. J. Hodson, N. Singh, J. H. Klootwijk, F. Roozeboom, M. C. M. van de Sanden and W. M. M. Kessels, Deposition of TiN and HfO_2 in a commercial 200mm remote plasma atomic layer deposition reactor, *J. Vac. Sci. Technol., A*, 2007, **25**(5), 1357–1366.

57 J. L. van Hemmen, S. B. S. Heil, J. H. Klootwijk, F. Roozeboom, C. J. Hodson, M. C. M. van de Sanden and W. M. M. Kessels, Plasma and Thermal ALD of Al_2O_3 in a Commercial 200 mm ALD Reactor, *J. Electrochem. Soc.*, 2007, **154**(7), G165–G169.

58 M. F. J. Vos, B. Macco, N. F. W. Thissen, A. A. Bol and W. M. M. Kessels, Atomic layer deposition of molybdenum oxide from $(NtBu)_2(NMe_2)_2Mo$ and O_2 plasma, *J. Vac. Sci. Technol., A*, 2016, **34**(1), 01A103.

59 N. H. Turner and A. M. Single, Determination of peak positions and areas from wide-scan XPS spectra, *Surf. Interface Anal.*, 1990, **15**(3), 215–222.

60 I. Alstrup, I. Chorkendorff, R. Candia, B. S. Clausen and H. Topsøe, A combined X-Ray photoelectron and Mössbauer emission spectroscopy study of the state of cobalt in sulfided, supported, and unsupported CoMo catalysts, *J. Catal.*, 1982, **77**(2), 397–409.

61 H. Li, Q. Zhang, C. C. R. Yap, B. K. Tay, T. H. T. Edwin, A. Olivier and D. Baillargeat, From Bulk to Monolayer MoS_2: Evolution of Raman Scattering, *Adv. Funct. Mater.*, 2012, **22**(7), 1385–1390.

62 A. Molina-Sánchez, K. Hummer and L. Wirtz, Vibrational and optical properties of MoS_2: From monolayer to bulk, *Surf. Sci. Rep.*, 2015, **70**(4), 554–586.

63 C. Lee, H. Yan, L. E. Brus, T. F. Heinz, J. Hone and S. Ryu, Anomalous Lattice Vibrations of Single- and Few-Layer MoS_2, *ACS Nano*, 2010, **4**(5), 2695–2700.

64 J. Jeon, S. K. Jang, S. M. Jeon, G. Yoo, Y. H. Jang, J. H. Park and S. Lee, Layer-controlled CVD growth of large-area two-dimensional MoS_2 films, *Nanoscale*, 2015, **7**(5), 1688–1695.

65 F. Dumeignil, D. Wang, E. W. Qian, S. Inoue, A. Muto, T. Kabe and A. Ishihara, Interpretation of the difference of optimal Mo density in MoS_2-Al_2O_3 and MoS_2-TiO_2 HDS catalysts, *Res. Chem. Intermed.*, 2005, **31**(9), 819–832.

66 S. Mignuzzi, A. J. Pollard, N. Bonini, B. Brennan, I. S. Gilmore, M. A. Pimenta, D. Richards and D. Roy, Effect of disorder on Raman scattering of single-layer MoS_2, *Phys. Rev. B: Condens. Matter Mater. Phys.*, 2015, **91**(19), 195411.

67 R. G. Dickinson and L. Pauling, THE CRYSTAL STRUCTURE OF MOLYBDENITE, *J. Am. Chem. Soc.*, 1923, **45**(6), 1466–1471.

68 S. Wang, Y. Rong, Y. Fan, M. Pacios, H. Bhaskaran, K. He and J. H. Warner, Shape Evolution of Monolayer MoS_2 Crystals Grown by Chemical Vapor Deposition, *Chem. Mater.*, 2014, **26**(22), 6371–6379.

69 S. Ghosh, K. Ganesan, S. R. Polaki, T. Mathews, S. Dhara, M. Kamruddin and A. K. Tyagi, Influence of substrate on nucleation and growth of vertical graphene nanosheets, *Appl. Surf. Sci.*, 2015, **349**, 576–581.

70 X. Zou and Y. Zhang, Noble metal-free hydrogen evolution catalysts for water splitting, *Chem. Soc. Rev.*, 2015, **44**(15), 5148–5180.

71 Y. Yang, H. Fei, G. Ruan, Y. Li and J. M. Tour, Vertically Aligned WS_2 Nanosheets for Water Splitting, *Adv. Funct. Mater.*, 2015, **25**(39), 6199–6204.

72 S. Shin, Z. Jin, D. H. Kwon, R. Bose and Y.-S. Min, High Turnover Frequency of Hydrogen Evolution Reaction on Amorphous MoS_2 Thin Film Directly Grown by Atomic Layer Deposition, *Langmuir*, 2015, **31**(3), 1196–1202.

73 S. Oh, J. B. Kim, J. T. Song, J. Oh and S.-H. Kim, Atomic layer deposited molybdenum disulfide on Si photocathodes for highly efficient photoelectrochemical water reduction reaction, *J. Mater. Chem. A*, 2017, **5**(7), 3304–3310.

74 E. Parzinger, E. Mitterreiter, M. Stelzer, F. Kreupl, J. W. Ager, A. W. Holleitner and U. Wurstbauer, Hydrogen evolution activity of individual mono-, bi-, and few-layer MoS_2 towards photocatalysis, *Appl. Mater. Today*, 2017, **8**, 132–140.

75 S. Li, S. Wang, M. M. Salamone, A. W. Robertson, S. Nayak, H. Kim, S. C. E. Tsang, M. Pasta and J. H. Warner, Edge-Enriched 2D MoS_2 Thin Films Grown by Chemical Vapor Deposition for Enhanced Catalytic Performance, *ACS Catal.*, 2017, **7**(1), 877–886.

76 C. Tsai, H. Li, S. Park, J. Park, H. S. Han, J. K. Nørskov, X. Zheng and F. Abild-Pedersen, Electrochemical generation of sulfur vacancies in the basal plane of MoS_2 for hydrogen evolution, *Nat. Commun.*, 2017, **8**, 15113.

77 H. Li, C. Tsai, A. L. Koh, L. Cai, A. W. Contryman, A. H. Fragapane, J. Zhao, H. S. Han, H. C. Manoharan, F. Abild-Pedersen, J. K. Norskov and X. Zheng, Activating and optimizing MoS_2 basal planes for hydrogen evolution through the formation of strained sulphur vacancies, *Nat. Mater.*, 2016, **15**(1), 48–53.